BUILDING AN ATLAS OF HIPPOCAMPAL SUBFIELDS USING POSTMORTEM MRI

Paul A. Yushkevich[1], *Brian B. Avants*[1], *John Pluta*[1,2], *David Minkoff*[1,2], *Stephen Pickup*[1], *Weixia Liu*[1], *John A. Detre*[1,2], *Murray Grossman*[2], and *James C. Gee*[1]

Departments of [1]Radiology and [2]Neurology, University of Pennsylvania, Philadelphia, PA, USA

ABSTRACT

This paper presents preliminary work on the construction of a computational anatomical atlas of the human hippocampus. The atlas is derived from high-resolution 9.4 Tesla MRI of postmortem samples. The main subfields of the hippocampus (cornu Ammonis fields CA1, CA2/3 and CA4; dentate gyrus; and the vestigial hippocampal sulcus) are labeled in the images manually using a combination of distinguishable image features and geometrical features. A synthetic average image is derived from the MRI of the samples using shape and intensity averaging in the diffeomorphic non-linear registration framework, and a consensus labeling of the template is generated. The agreement of the consensus labeling with manual labeling of each sample is measured, and the effect of aiding registration with landmarks and manually generated mask images is evaluated.

Index Terms— Brain, hippocampus, image registration, magnetic resonance imaging

1. INTRODUCTION

The hippocampus is a structure of acute interest in neuroimaging. It is the principal component of the declarative memory system [1] and is of vital interest in the study of dementia, epilepsy and other neurological and psychiatric disorders. The hippocampus has a complex shape, being formed by two folding interlocking layers: *cornu Ammonis (CA)* and *dentate gyrus (DG)*. Hippocampal layers and the subfields into which they are further divided serve different functions. Non-uniform neuron loss across the hippocampus has been reported in neurodegenerative disorders [2], as has a non-uniform rate of neuroplasticity [3]. However, the boundaries between CA and DG are practically impossible to distinguish in clinical MRI, except when using T2 weighting with highly anisotropic voxels [4]. Thus, it is common to represent the hippocampus as a homogeneous blob-like structure with a large head and a curved tail.

The aim of this work is to build an anatomical atlas of the hippocampus that accurately describes the distribution and the shape of its main subfields. The applications of such an atlas would include *in vivo* imaging studies aimed at detecting structural and functional differences across the hippocampal subfields in the context of neurodegenerative disease. A few recent studies have sought such differentiation, but relied on direct labeling of the hippocampus in *in vivo* MRI [5, 6, 4] or labeling of geometric templates derived from *in vivo* imaging [7]. We believe that a detailed hippocampus atlas based on high-resolution postmortem imaging would prove highly complementary to these studies.

Our approach involves MRI of brain samples containing the intact whole hippocampus at 9.4 Tesla, using overnight scans to achieve good contrast at high resolution. While others have imaged portions of the hippocampus at even higher resolution [8], to the best of our knowledge, this is the first work to collect images of the entire structure with isotropic or nearly isotropic voxels around 0.01mm^3 in volume. We manually label hippocampal subfields relying on a combination of discernable intensity and shape features. To combine data from different samples, we apply unbiased image averaging [9] based on diffeomorphic Lagrangian frame image registration. Registration accuracy is evaluated in terms of subfield label alignment in atlas space.

Our atlas is a work in progress, with only five hippocampi imaged so far. However, we believe that this paper establishes a viable pipeline for achieving our goal of building a larger atlas from 20 or more tissue samples.

2. METHODS AND MATERIALS

2.1. Specimens and Imaging

Formalin-fixed brain specimens ($\geq$21 days) from autopsy cases with no abnormal neuropathological findings were studied. Hemispheres were separated from the cerebellum and brain stem and samples containing the intact hippocampus and able to fit inside of a $70mm$ diameter MRI coil were extracted from each hemisphere by making two incisions: the first, orthogonal to the midsagittal plane and parallel to the main axis of the hippocampus, passing through the corpus callosum; the second, parallel to the midsagittal plane, removing the lateral-most third of the sample.

Imaging took place on a 9.4 Tesla Varian 31cm horizon-

This project is supported by NIH grants AG027785, NS061111, MH068066 and NS045839, the McCabe Foundation Pilot Award and the Pilot Project Award from the Penn Comprehensive Neuroscience Center.

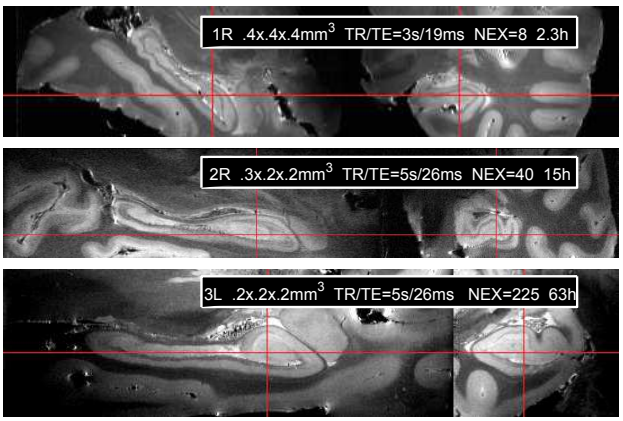

Fig. 1. Images of three hippocampus samples with different voxel sizes and MRI acquisition parameters.

tal bore scanner (Varian Inc, Palo Alto, CA) using a 70mm ID TEM transmit/receive volume coil (Insight Neuroimaging Systems, Worchester, MA). Samples were placed in leak-proof bags and wrapped with plastic to fit snugly inside the coil. We used a multi-slice spin echo sequence with TR/TE = 5s/25ms and 0.2mm slice thickness. An oblique slice plane was chosen to cover the hippocampus with as few slices as possible (around 130 slices for most images). The phase encode direction was from left to right and the readout direction followed the long axis of the hippocampus. The field of view was typically $60\text{mm} \times 90\text{mm}$, with matrix size 300×300, yielding 3D images of $0.2\text{mm} \times 0.3\text{mm} \times 0.2\text{mm}$ resolution. Samples were scanned over $12 - 16$ hours with 32-44 averages. One sample was scanned at $(0.2\text{mm})^3$ resolution with 225 averages over 63 hours.

2.2. Manual Segmentation

Reconstructed MRI images were segmented by one of the authors (JP) using the Duvernoy atlas as a reference [10]. The layered structure of the hippocampus is clearly visible in these images (Fig. 1). The most distinct features are the outer boundary of CA and the dark layer consisting of the vestigial hippocampal sulcus (VHS) and stratum radiatum (SR). The boundaries between the DG, the VHS on one side, and the inner portion of CA on the other, are also visible in many locations. The boundaries between the subfields of the CA, and between CA1 and the adjacent subiculum are not visible, and the separation has to be made based on position and shape, rather than intensity.

Tracing was performed in three orthogonal view planes using ITK-SNAP (itksnap.org). Five subfields were labeled: CA1, CA2 combined with CA3, CA4, VHS combined with SR and DG. Most of the time was spent labeling in the coronal plane, with verification in the sagittal plane. Segmentation is very labor-intensive, requiring about 20-40 person-hours, depending on the resolution of the images.

2.3. Atlas Generation

Combining image data from multiple samples into a common atlas allows us to generate a model of "average" hippocampal anatomy, to boost signal-to-noise ratio, and to study variations in hippocampal structure across subjects. In building an atlas, we follow the work of Guimond and others [11, 12, 9] by searching for a synthetic image that can be nonlinearly registered to each of the input images with minimal total deformation. Registration follows the *Symmetric Normalization (SyN)* framework [13]. Given an image match metric Π, registration of images I and J seeks a pair of diffeomorphic maps ϕ_1, ϕ_2 that minimize

$$\begin{aligned} E(I, J, \phi_1, \phi_2) = \Pi[I(\phi_1(\mathbf{x}, \frac{1}{2})), J(\phi_2(\mathbf{x}, \frac{1}{2}))] \quad + \\ + \quad \int_0^{\frac{1}{2}} \|\vec{v}_1(\mathbf{x}, t)\|_L \, \mathrm{d}t + \int_0^{\frac{1}{2}} \|\vec{v}_2(\mathbf{x}, t)\|_L \, \mathrm{d}t \quad , \\ \text{subj. to } \frac{\partial \phi_i(\mathbf{x}, t)}{\partial t} = \vec{v}_i(\phi_i(\mathbf{x}, t), t) \, , \quad i = 1, 2 \, . \end{aligned} \quad (1)$$

Symmetric diffeomorphic maps from I to J and from J to I are given, respectively, by $\phi_2^{-1} \circ \phi_1$ and $\phi_1^{-1} \circ \phi_2$.

Registration of postmortem MRI is challenging because images have different fields of view and because there are many unique local intensity features in each image (vessels, hyperintensities, imaging artifacts) that make finding one-to-one correspondences difficult. To boost registration accuracy, we introduce two kinds of manually generated aids: landmarks and rough binary masks of the hippocampus. Landmarks are placed at the two ends of each digitation in the head of the hippocampus (digitations are folds that can be seen in the right column of Fig. 1), as well as at the anterior-most point of the head and posterior-most point of the tail. Binary masks are drawn in the axial plane, where the hippocampus occupies the fewest number of slices. Both types of aids can can be generated in about an hour, and, in the context of a larger study, it is much more cost-effective to generate these aids than full manual segmentations.

Initial linear alignment of hippocampus images proved particularly difficult. Approaches based on image forces alone would often get stuck in local minima, yielding nonsensical results. Thus, affine alignment was performed by landmark matching, followed by matching of binary masks. Subsequent atlas building involved the following algorithm [9]: (1) use SyN to register every image to a template; (2) average the intensity of all registered images; (3) average the initial velocity fields $\vec{v}(\mathbf{x}, 0)$ of the maps from the template to each of the images and generate a shape distance minimizing diffeomorphic update to the template shape; this step is known as shape averaging [9]; (4) repeat step 1 using the new shape average as the template. To make group-wise registration unbiased, Avants et al. [9] suggest using the intensity average of affine-registered images as the initial template. However, this requires a substantial number of images, so

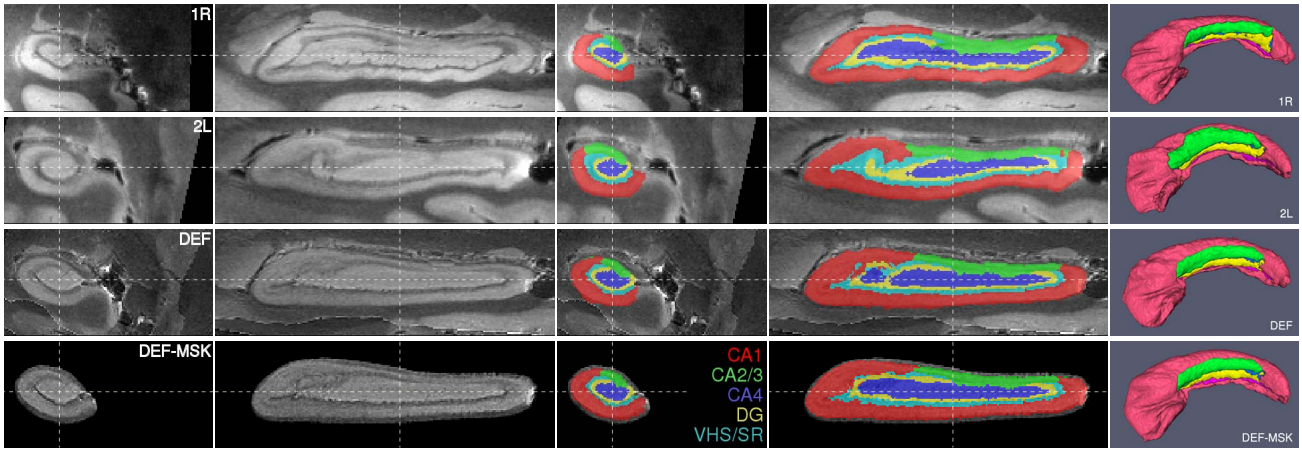

Fig. 2. Coronal, sagittal and 3D views of hippocampus images and subfield labels for samples 1R and 2L, following affine alignment, and for atlases computed by unsupervised deformable registration (DEF) and mask-aided registration (DEF-MSK). Abbreviations: CA - cornu Ammonis; DG - dentate gyrus; VHS - vestigial hippocampal sulcus; SR - stratus radiatum.

that the features common to all images are more prominent than the variation across images. Since in our case the number of samples is small, we choose one of the samples as the initial template. We use the normalize cross-correlation image match metric, which is robust to intensity inhomogeneity present in our data.

A consensus segmentation of the atlas is generated by warping the manual segmentations to the atlas and using the STAPLE algorithm [14] to assign a label to each voxel. To examine the quality of alignment, we report the overlap in template space between the STAPLE segmentation and each of the individual segmentations.

3. RESULTS

Fig. 1 shows three samples scanned with different protocols to illustrate the effect of resolution (the lower-resolution $(0.4\text{mm})^3$ image was not used for atlas building). These images have good contrast, and the edges separating the hippocampus from adjacent tissue are well pronounced (e.g., unlike in clinical MRI, the amygdala is clearly separated from the hippocampus). A number of imaging artifacts are also evident: intensity inhomogeneity; hyperintensity and small amounts of distortion at tissue-air boundaries; ringing and motion artifacts are also present in some images.

Segmentation results for two of the samples are shown in Fig. 1, along with two of the atlases generated by diffeomorphic averaging. Notice that the atlas has image characteristics and shape similar to that of the input images. This is particularly noticeable in the 3D renderings of STAPLE segmentations, where the digitations in the head of the hippocampus are clearly visible.

For each subfield, Fig 3 plots the average Dice overlap between the STAPLE segmentation in atlas space and warped individual segmentations. Overlap is as high as 90% for CA1, which is the largest subfield and 80% for CA4, which is smaller, but also the least hollow of the subfields. For other subfields, overlap is only 60% to 70%. However, since these subfields are very thin, even a small misalignment results in large overlap error. The improvement given by deformable registration over affine alignment is clear, while the benefit of masks and landmarks is limited. Landmarks, in fact, lead to slightly reduced overlap, while masks slightly boost overlap in CA1 and CA4 at the cost of an even slighter decrease in the overlap of the smaller structures.

4. DISCUSSION

While the techniques described above can be readily used for MRI-based postmortem morphometry, a higher impact would be achieved if the atlas were to be applied to *in vivo* imaging studies, such as longitudinal studies of subfield-level atrophy in neurodegenerative disorders or analysis of differences in fMRI activation across subfields. For this to be possible, we need a way to register the postmortem hippocampus atlas to *in vivo* MRI. The thin-slice T2-weighted turbo spin echo protocol used by [4, 6] presents a good registration target since the dark band formed by the VHS, SR and DG is partially visible in such images. Another potential application is to guide automatic model-based segmentation, where we expect a richer prior model of hippocampus shape to achieve better segmentation accuracy.

When applying the postmortem atlas to *in vivo* data, one must be cautious to account for morphological differences between the living brain and formalin-fixed samples. Cutting of the samples may introduce additional deformations, although we take care to leave at least 1cm of tissue around the hippocampus to reduce such distortion. Nevertheless, some form

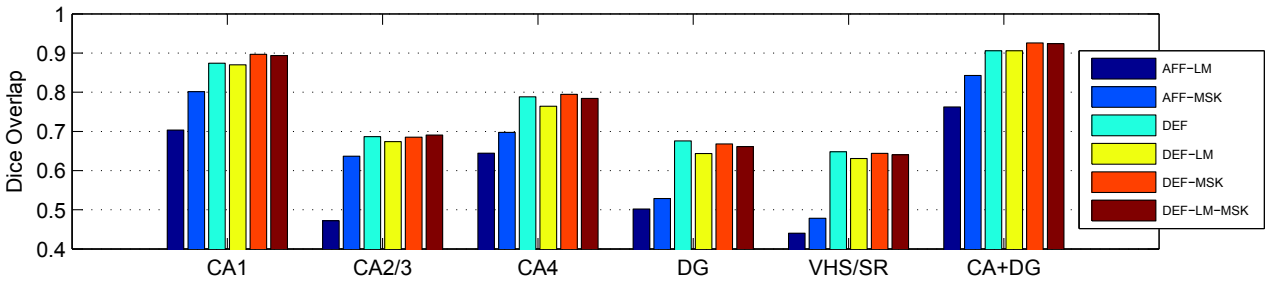

Fig. 3. Agreement between the consensus atlas labeling and segmentation of individual samples expressed in terms of average Dice overlap computed in atlas space. Six atlas-building approaches are compared: landmark-based and mask-based affine alignment (AFF-LM / AFF-MSK), image-based deformable normalization (DEF), deformable normalization aided by landmarks (DEF-LM), masks (DEF-MSK) and both masks and landmarks (DEF-LM-MSK).

of global shape correction will likely be necessary to account for these differences.

5. REFERENCES

[1] L. R. Squire, "Memory and the hippocampus: a synthesis from findings with rats, monkeys, and humans," *Psychol Rev*, vol. 99, no. 2, pp. 195–231, 1992.

[2] Mark J West, Claudia H Kawas, Walter F Stewart, Gay L Rudow, and Juan C Troncoso, "Hippocampal neurons in pre-clinical alzheimer's disease.," *Neurobiol Aging*, vol. 25, no. 9, pp. 1205–1212, Oct 2004.

[3] P. S. Eriksson, E. Perfilieva, T. Bjrk-Eriksson, A. M. Alborn, C. Nordborg, D. A. Peterson, and F. H. Gage, "Neurogenesis in the adult human hippocampus.," *Nat Med*, vol. 4, no. 11, pp. 1313–7, Nov 1998.

[4] Michael M Zeineh, Stephen A Engel, Paul M Thompson, and Susan Y Bookheimer, "Dynamics of the hippocampus during encoding and retrieval of face-name pairs.," *Science*, vol. 299, no. 5606, pp. 577–80, Jan 2003.

[5] C. Brock Kirwan, Craig K Jones, Michael I Miller, and Craig E L Stark, "High-resolution fmri investigation of the medial temporal lobe.," *Hum Brain Mapp*, vol. 28, no. 10, pp. 959–966, Oct 2007.

[6] Susanne G. Mueller, Norbert Schuff, Sky Raptentsetsang, Lara Stables, and Michael W. Weiner, "Distinct atrophy pattern in hippocampal subfields in Alzheimers disease (AD) and mild cognitive impairment (MCI)," *Alzheimer's and Dementia*, vol. 3, no. 3, pp. S113, 2007.

[7] Lei Wang, J. Philp Miller, Mokhtar H Gado, Daniel W McKeel, Marcus Rothermich, Michael I Miller, John C Morris, and John G Csernansky, "Abnormalities of hippocampal surface structure in very mild dementia of the Alzheimer type.," *Neuroimage*, vol. 30, no. 1, pp. 52–60, Mar 2006.

[8] Girish M Fatterpekar, Thomas P Naidich, Bradley N Delman, Juan G Aguinaldo, S. Humayun Gultekin, Chet C Sherwood, Patrick R Hof, Burton P Drayer, and Zahi A Fayad, "Cytoarchitecture of the human cerebral cortex: MR microscopy of excised specimens at 9.4 Tesla.," *AJNR Am J Neuroradiol*, vol. 23, no. 8, pp. 1313–1321, Sep 2002.

[9] Brian Avants and James C Gee, "Geodesic estimation for large deformation anatomical shape averaging and interpolation.," *Neuroimage*, vol. 23 Suppl 1, pp. S139–S150, 2004.

[10] H. M. Duvernoy, *The human hippocampus, functional anatomy, vascularization and serial sections with MRI*, Springer, third edition edition, 2005.

[11] Alexandre Guimond, Jean Meunier, and Jean-Philippe Thirion, "Average brain models: a convergence study," *Comput. Vis. Image Underst.*, vol. 77, no. 9, pp. 192–210, 2000.

[12] Brad Davis, Peter Lorenzen, and Sarang C. Joshi, "Large deformation minimum mean squared error template estimation for computational anatomy.," in *Proc. IEEE International Symposium on Biomedical Imaging*, 2004, pp. 173–176.

[13] B. B. Avants, C. L. Epstein, M. Grossman, and J. C. Gee, "Symmetric diffeomorphic image registration with cross-correlation: Evaluating automated labeling of elderly and neurodegenerative brain.," *Med Image Anal*, Jun 2007, In press.

[14] Simon K Warfield, Kelly H Zou, and William M Wells, "Simultaneous truth and performance level estimation (STAPLE): an algorithm for the validation of image segmentation.," *IEEE Trans Med Imaging*, vol. 23, no. 7, pp. 903–921, Jul 2004.